NATIONAL ADVISORY COMMITTEE FOR AERONAUTICS

TECHNICAL NOTE 3306

AN INVESTIGATION OF A LIFTING 10-PERCENT-THICK SYMMETRICAL DOUBLE-WEDGE AIRFOIL AT MACH NUMBERS UP TO 1

By Milton D. Humphreys

Langley Aeronautical Laboratory
Langley Field, Va.

Washington
November 1954

NATIONAL ADVISORY COMMITTEE FOR AERONAUTICS

TECHNICAL NOTE 3306

AN INVESTIGATION OF A LIFTING 10-PERCENT-THICK SYMMETRICAL DOUBLE-WEDGE AIRFOIL AT MACH NUMBERS UP TO 1

By Milton D. Humphreys

SUMMARY

Pressure measurements on the surface of a two-dimensional symmetrical double-wedge airfoil have been obtained from tests in the Langley 4- by 19-inch semiopen tunnel at lifting conditions and at Mach numbers up to 1. The object of this investigation was to obtain normal-force, pressure-drag, and pitching-moment data and to compare them with available experimental and theoretical results.

The nonlifting results are in good agreement with potential-flow theory at a Mach number of about 0.5 and in fair agreement with the theoretical results of Guderley and Yoshihara at a Mach number of 1 and with the transonic small-disturbance theories of other investigators for Mach numbers from 0.85 to 1.0.

Below a reduced Mach number ξ_0 of approximately -1.0, the pressure-drag coefficient computed on the basis of the transonic theories and the drag coefficient measured in the present investigation are of opposite sign. The present experimental data and the theoretical incompressible results extended to high-subsonic speeds both indicate a thrust for the forebody. The application of transonic approximations, therefore, appears unjustified for similarity parameters less than approximately -1.0 in the subsonic portion of the transonic range.

At lifting conditions, for Mach numbers up to about 0.6, the present results are in good agreement with the closed-tunnel data of Bartlett and Peterson and with low-speed theoretical data extended to a Mach number of 0.6.

INTRODUCTION

Among airfoil profiles, the wedge is of particular interest, since its geometric simplicity permits ready formulation of a problem with known boundary conditions in the hodograph plane. Consequently, it has been the subject of considerable theoretical work in the transonic Mach number range. Guderley and Yoshihara (ref. 1) first obtained a solution to the problem of the flow past a thin double-wedge profile at 0° angle

of attack and a Mach number of 1. Trilling (ref. 2) has also made an analytical study of steady plane flow of an ideal gas past a thin, symmetrical double-wedge profile at 0° angle of attack at transonic Mach numbers. Previously reported experimental investigations (refs. 3 and 4) have provided data on 10-percent-thick symmetrical double-wedge airfoils at 0° angle of attack and transonic Mach numbers.

Recently, Guderley and Yoshihara (ref. 5) have obtained theoretical results for a symmetrical double-wedge profile under lifting conditions at a Mach number of 1. A survey of the experimental data for the double-wedge profile reveals that only one investigation (ref. 6) has been made at lifting conditions and it covered only Mach numbers below 0.85. The present results are compared with available theoretical and experimental results for both the lifting and nonlifting conditions. Pressure-distribution, normal-force-curve-slope, pressure-drag, and pitching-moment data are presented.

The data were obtained in the form of pressure distributions and schlieren flow photographs for the profile at angles of attack of 0°, 4°, and 8° at Mach numbers from 0.3 to 1.0. The Reynolds number range was from 0.7×10^6 to 1.6×10^6.

SYMBOLS

c	airfoil chord
c_d	section drag coefficient, $c_{d_p} + 0.006$
c_{d_p}	section pressure-drag coefficient
$\tilde{c}_d$	generalized section pressure-drag coefficient, $\frac{\left[M^2(\gamma + 1)\right]^{1/3} c_{d_p}}{(t/c)^{5/3}}$
$c_{m_{LE}}$	section moment coefficient about the leading edge
c_n	section normal-force coefficient
d	section drag
h	tunnel height
M	free-stream Mach number

ξ_o reduced Mach number, $\dfrac{M^2 - 1}{\left[(\gamma + 1)\dfrac{M^2 t}{c}\right]^{2/3}}$

n section normal force

P pressure coefficient, $\dfrac{p_l - p}{q}$

P_{cr} critical pressure coefficient (for local $M = 1.0$)

P_o pressure coefficient derived from potential-flow theory (at $M = 0$)

p free-stream static pressure

p_l local static pressure

q free-stream dynamic pressure

t thickness

t/c airfoil thickness ratio

x distance along chord

α angle of attack, deg

γ ratio of specific heats (1.4 for air)

APPARATUS, MODELS, AND TESTS

Tests were conducted in the Langley 4- by 19-inch semiopen tunnel, shown in figure 1. In this facility air from the atmosphere is induced to flow through the test section by a high-pressure induction nozzle. The test-section Mach number was regulated by a variable-area throat located in the diffuser downstream from the test section. This variable-area throat, by maintaining sonic velocity at the throat for all test-section Mach numbers, permitted continuous control of an undisturbed flow in the test section at Mach numbers from 0.3 to 1.0. The tunnel Mach number was obtained from calibrated orifices in the open chambers above and below the test section.

For incompressible potential flow the correction to the angle of attack is the major correction and is given (for the tunnel configuration used) by $\alpha_{true} = \alpha_{test} - 1.85c_n$. Jet-boundary corrections for

this tunnel configuration have not yet been determined at high subsonic Mach numbers; therefore no correction has been applied to any of these data, except in one instance, where the incompressible correction was applied to the normal-force-curve-slope results at low Mach numbers. Jet-boundary effects at low Mach numbers are discussed in more detail in reference 7, where it is indicated that, except for the angle-of-attack correction, the jet-boundary effects are probably not large.

The 10-percent-thick symmetrical double-wedge airfoil (maximum t/c at 0.5c), having a 4-inch chord and 4-inch span (see fig. 2), completely spanned the test section and was supported by circular end plates in the tunnel walls (fig. 1). Static-pressure orifices were located at 5-percent-chord intervals along the upper and lower surfaces of the airfoil (fig. 2).

Pressure-distribution tests and schlieren flow photographs were made for the airfoil at angles of attack of 0°, 4°, and 8° and at Mach numbers from 0.3 to 1.0. The corresponding Reynolds number range for the 4-inch-chord model was from 0.7×10^6 to 1.6×10^6.

RESULTS AND DISCUSSION

Comparison of Theoretical and Experimental Data

Pressure-distribution comparisons.- Figure 3 presents a comparison of experimental pressure distributions of the present work and of references 3 and 4 with the theoretical pressure distributions of reference 1 for 10-percent-thick symmetrical double-wedge sections at 0° angle of attack and Mach number 1.0. Over the forward half of the airfoil the experimental pressure distribution from the Langley 4- by 19-inch semi-open tunnel shows lower pressures than either the theoretical data of reference 1 or the experimental data of references 3 and 4, the data of reference 4 following the theoretical curve, while the data of reference 3 show higher pressures than the other results. Over the rear half of the profile the data of the present investigation show closer agreement with the theoretical distribution than the data of references 3 and 4. The data of reference 3 again show much higher pressures than any of the other theoretical or experimental results.

The data of the current investigation at 0° angle of attack and a Mach number of 0.584 are compared in figure 4 with the theoretical potential-flow pressure distribution extrapolated from $M = 0$ to $M = 0.584$, using the Von Kármán-Tsien relation. The pressure distributions from the current tests are in very good agreement with theory, although they are generally somewhat higher.

A comparison of pressure distributions obtained in the present investigation (c/h = 0.21) with two-dimensional data obtained for a 3-inch-chord 10-percent-thick symmetrical double-wedge airfoil in a 4- by 16-inch closed-throat high-speed wind tunnel having a c/h ratio of 0.187 (ref. 6) at high subsonic speeds and at two lifting conditions is shown in figure 5. The agreement shown between the pressure-distribution data near zero normal-force coefficient at a Mach number of approximately 0.7 is excellent. Under lifting conditions, with normal-force coefficients near 0.68 and at a Mach number of about 0.75, some slight discrepancies are in evidence but the agreement is generally satisfactory.

Pressure-drag comparisons.- A comparison of drag polars in figure 6 shows reasonably good agreement between the data of the present investigation and reference 6 for Mach numbers through 0.7. At a Mach number of 0.8 the drag data of the reference paper are somewhat higher, perhaps due to the nearness to the choke Mach number of 0.851 in the closed-throat-tunnel data of reference 6.

The zero-lift experimental pressure-drag coefficients of a 10-percent-thick symmetrical double-wedge airfoil from the Langley 4- by 19-inch semiopen tunnel are compared with data obtained from references 4 and 6, and with the theoretical data from references 1, 2, and 8 in figure 7. For Mach numbers up to 0.8 the theoretical data of reference 2 are generally much higher than those shown for the experimental investigations. The present investigation shows lower drag coefficients at these Mach numbers than any of the other investigations, while references 4 and 6 show values between the present results and the theory of reference 2. At Mach numbers around 0.8 the experimental data of reference 6 show a sharp rise and have higher values than the theoretical curve. The high drag coefficients shown at and above that Mach number are attributed to the nearness to the choke Mach number of 0.851 in the closed-throat-tunnel data of reference 6. Generally, fair agreement exists between the theoretical and the experimental results at Mach numbers from 0.85 to near 1. The slightly negative slope of the drag curve at a Mach number of 1 from the present investigation is in conformity with the results given previously in reference 8.

The components of drag acting on a 10-percent-thick symmetrical double-wedge airfoil at 0° incidence are shown in figure 8. The drag coefficient on the forebody rises uniformly with Mach number and continues to increase through a Mach number of 1. While the drag of the afterbody rises more rapidly with Mach number than does the forebody drag, the afterbody drag reaches a maximum somewhat below a Mach number of 1 and then decreases with further increase in Mach number. The slopes of the drag curve with Mach number at a Mach number of 1 are in agreement with predicted slopes from reference 8. Further, the pressure-drag-coefficient curves are also in fair agreement with

Guderley's theoretical values at a Mach number of 1 and with pressure-drag values from theoretical incompressible pressure-distribution results extended to a Mach number of 0.480 by the Von Kármán-Tsien rule.

Below a Mach number of 0.85, the drag coefficient for the forebody is negative, as shown by the present experimental data and by theory. The negative drag of the forebody of the symmetrical double-wedge profile at Mach numbers below 0.85 is produced by the large area of the forebody affected by pressures lower than that of the stream. For instance, figure 4 indicates that zero pressure coefficient occurs near the 16-percent-chord station at a Mach number of 0.584 and is near the midchord location at a Mach number of 1. A gradual rearward movement of the chordwise position of zero pressure coefficient necessarily occurs, as will be shown later in the discussion. Thus, the negative drag produced on the forebody diminishes with increasing Mach number and the drag becomes positive at Mach numbers above 0.85 (fig. 8).

Figure 9 shows, in transonic-similarity terms, the drag data at zero lift for the forebody of the 10-percent-thick symmetrical double-wedge model of the present investigation compared with similar drag data on wedges from the experimental investigations of references 4 and 9 and the theoretical results of references 1, 2, 8, and 10. To provide better data correlation, the similarity parameters have been modified by using $(\gamma + 1)M^2$, rather than the term $\gamma + 1$ in these parameters in accordance with the suggestion of Busemann in reference 11 and the subsequent use by other investigators. At sonic speeds (figs. 8 and 9), the slopes are in reasonably good agreement with the theory from reference 8. Agreement is maintained with the theories (refs. 2 and 10) from Mach number 1.0 to around 0.85 ($\xi_0 = 0$ to $\xi_0 \approx -1.0$). Below a reduced Mach number ξ_0 of approximately -1.0, the pressure-drag coefficient computed on the basis of the transonic theories and the drag coefficient measured in the present investigation are of opposite sign. The present experimental data and the theoretical incompressible results extended to high-subsonic speeds (fig. 8) both indicate a thrust for the forebody. The application of transonic approximations used in references 2 and 10, therefore, appears unjustified for similarity parameters ξ_0 less than approximately -1.0 in the subsonic portion of the transonic range. The fact that the transonic small-disturbance theories do not apply at the lower values of the reduced Mach number could be expected because the transonic theory becomes linear theory at the lower Mach numbers and approaches zero drag coefficient as a limit. The limitation could be expected from Busemann's discussion of the application of the transonic similarity rules in reference 11.

The data of reference 4 were obtained in a 1/8-open slotted tunnel in which the model size relative to the tunnel height was of extremely large proportions, the c/h ratio being 0.89. In view of the fact

that quantitative evaluation of the jet-boundary-interference corrections was not made in the reference paper, the agreement between the uncorrected results from the two facilities is as good as can be expected.

Bryson's measurements (ref. 9) follow the trend predicted by transonic-similarity theory and thus also do not indicate negative drag at the lower values of the reduced Mach number. The difference between the current tests and Bryson's data is primarily attributed to model differences. The wedge of reference 9 was attached to a flat-plate extension constituting an afterbody of uniform thickness equal to the maximum thickness of the wedge, while the present results were obtained on the wedge forebody of a symmetrical double-wedge airfoil. A comparison (fig. 10) of the experimental pressure distribution for the 5.74° semiangle forebody of the present investigation with an interpolated distribution for a 5.74° semiangle wedge from reference 9 ($M \approx 0.82$) shows that, while the interpolated pressures are generally higher than those from the present tests, they are considerably higher near the nose and near the shoulder. The higher pressures produce the higher drag shown for the data of reference 9. The fairing of the pressure distribution in the neighborhood of the shoulder of the airfoil can be made by either of the following methods: (1) the fairing can be made to pass through the pressure coefficient measured at the shoulder of the airfoil; (2) the pressure distribution can be faired through the theoretical value of the pressure coefficient at the shoulder (that is, the pressure coefficient corresponding to sonic velocity at the shoulder of a double-wedge profile). In the present investigation the former method was used, since it is known that, due to the boundary layer, the sonic-velocity point is forward of the shoulder and the measured pressure must be used to give a realistic estimate of the drag forces. Had the fairings and drag integrations been made on the assumption that the theoretical sonic-velocity point occurred at the shoulder of the double-wedge airfoil (indicated by the long-dash line extension of the present data to $P = -0.41$ in fig. 10), the drag coefficients would have been somewhat increased and the Mach number at which the forebody drag became zero would have been reduced by a small amount.

A comparison of experimental and theoretical results indicates that low-speed theoretical data extended to Mach number 0.480 are in good agreement with the present experimental results. At Mach numbers from 0.85 to 1.0, similar agreement is obtained between experimental results and the transonic theories. Below a reduced Mach number ξ_0 of approximately -1.0, the pressure-drag coefficient computed on the basis of the transonic theories and the drag coefficient measured in the present investigation are of opposite sign. The present experimental data and the theoretical incompressible results extended to high-subsonic speeds both indicate a thrust for the forebody. The application of the transonic approximations, therefore, appears unjustified for similarity parameters ξ_0 less than approximately -1.0 in the subsonic portion of the transonic range.

Experimental Results

Schlieren photographs and pressure distributions.- Figure 11 presents schlieren flow photographs with superimposed pressure distributions for the airfoil at angles of attack of 0°, 4°, and 8° and Mach numbers of 0.7, 0.8, 0.9, and 1.0. Additional pressure-coefficient data are given in table I. The schlieren photographs and pressure distributions indicate that supersonic velocities occur near the shoulder of the wedge at a Mach number of 0.7 at 0° angle of attack. The pressure distributions (see also fig. 4) show that velocities greater than the stream velocity occur near the 16-percent-chord station at 0° angle of attack at a Mach number of 0.584 and move rearward to a position very near the shoulder of the wedge at a Mach number of 1. This phenomenon produces the rise in c_{d_p} of the forebody with increasing Mach number. As a Mach number of 1 is approached, the shock moves to the trailing edge, separation is eliminated, and an essentially constant supersonic velocity exists over the entire rear half of the model. The flow over the forward part of the wedge profile is subsonic.

At 4° angle of attack, at the lower Mach numbers, the flow separates at the nose and at the shoulder of the wedge. As the Mach number is increased above 0.8, the flow attaches to the leading edge and the shocks move rearward. The load reversal on the rear of the model at a Mach number of 0.9 produces a loss in lift and an increase in the positive pitching-moment coefficient. At a Mach number of 1 the flow is of the supersonic type, with the shocks at the trailing edge and very little separation existing on the rear of the model.

At 8° angle of attack the flow conditions are similar to those observed at 4° angle of attack, except that the negative pressure peaks are higher, the flow separation more extensive, and the shocks much stronger than for the lower angle-of-attack condition. From the pressure-distribution diagrams it is apparent that a very large portion of the total normal force is produced on the forebody of the symmetrical double-wedge airfoil and the flow changes on the afterbody produce large force and moment changes at transonic Mach numbers.

Section normal force.- The pressure-distribution diagrams were integrated to provide the basic aerodynamic characteristics for the 10-percent-thick symmetrical double-wedge airfoil and are shown as the c_n, c_d, and $c_{m_{LE}}$ variations with Mach number in figure 12. The normal-force-coefficient curves (fig. 12), generally similar to conventional airfoil data, rise according to subsonic theory, reaching a peak value around a Mach number of 0.8 and a minimum value near 0.9. The change is shown by figure 11 to result from the flow separation and consequent lift reversal over the rear of the airfoil. The recovery of lift at Mach numbers increasing from 0.9 to 1.0 is caused by the

movement along the upper surface of the shock wave and separation point to the trailing edge and the elimination of the load reversal over the rear of the airfoil.

Presented in figure 13 are both the uncorrected normal-force-curve-slope data of the present investigation for Mach numbers from 0.4 to 1.0 and the data corrected at Mach numbers from 0.4 to 0.65 for the incompressible jet-boundary effects using the relation $\alpha_{true} = \alpha_{test} - 1.85c_n$ (ref. 7). The data of the present investigation are also compared in figure 13 with the theoretical value at a Mach number of 1 from reference 5 and with the experimental data of reference 6. The latter results have been corrected for jet-boundary effects by the method of reference 12. The corrected normal-force-curve slopes of the current investigation are somewhat higher than those of the reference data. At a Mach number of 1 the agreement of the present uncorrected data with the theoretical results of reference 5 is close; however, this agreement may be only fortuitous, since the experimental data are subject to jet-deflection correction of roughly 20 percent at Mach numbers around 0.65 and of unknown magnitude at higher subsonic and transonic Mach numbers. Nevertheless, the data of figure 13 establish the trend of the normal-force-curve slope at Mach numbers up to 1.

Section moment coefficient about the leading edge.- The flow changes over the rear of the model (fig. 11), similar to their effect on the normal-force coefficient, produce large changes in the moment coefficient with Mach number for Mach numbers from 0.8 to 1.0 (fig. 12). A large reduction occurs in the negative pitching-moment coefficient for the model when the Mach number increases from 0.85 to 0.9. Above a Mach number of 0.9, the moment coefficient increases sharply. This severe change in the moment coefficient in the range of Mach numbers from 0.85 to 1 could produce serious stability and control problems for aircraft using symmetrical double-wedge sections at these Mach numbers. The variation of $dc_{m_{LE}}/dc_n$ with Mach number is shown in figure 14.

Section drag coefficient.- Figure 12 presents the variations of section drag with Mach number for 0°, 4°, and 8° angle of attack. To approximate the section drag, a skin-friction-drag coefficient of 0.006 has been added to the pressure-drag coefficients obtained from integrated chordwise pressure distributions. For subsonic Mach numbers up to around 0.8, large drag increases are produced by increases in the angle of attack. These drag increments are rather large because of the extensive flow separation from the nose and shoulder of the model occurring at the lower Mach numbers (see fig. 11). As the Mach number is increased above 0.8, however, the effect of increased angle of attack or normal force in producing increases in drag is considerably reduced because of the alleviation of separation by flow attachment at the nose. Figure 15 shows a reduction in the slope of the drag polars for low normal-force coefficients with increasing Mach numbers. This reduction in

slope is caused not only by the effect of Mach number on $\Delta c_d/\Delta\alpha$, but also includes the effects of Mach number on the normal-force coefficient. The overall effect of increasing the Mach number on the efficiency of the 10-percent-thick symmetrical double wedge is shown in the n/d curves of figure 16. Reduction in n/d ratio occurs with increase in Mach number from 0.6 to 0.9. Above 0.9, there is little change with Mach number in the n/d curves for the 10-percent-thick symmetrical double-wedge model. Figure 17 shows the variation with Mach number of the ratio of maximum normal force to drag for the symmetrical double-wedge airfoil and for a conventional NACA 64A012 airfoil (from unpublished data). A comparison of the values of $(n/d)_{max}$ for the two airfoils shows, as would be expected, that the symmetrical double-wedge airfoil has much lower maximum n/d values than the conventional section at Mach numbers below 0.85. Above a Mach number of 0.85, the value of $(n/d)_{max}$ is about the same for both airfoils.

CONCLUSIONS

The nonlifting results are in good agreement with potential-flow theory at a Mach number of approximately 0.5 and in fair agreement with the theoretical results of Guderley and Yoshihara at a Mach number of 1 and with the transonic small-disturbance theories of other investigators for Mach numbers from 0.85 to 1.0.

Below a reduced Mach number ξ_0 of approximately -1.0, the pressure-drag coefficient computed on the basis of the transonic theories and the drag coefficient measured in the present investigation are of opposite sign. The present experimental data and the theoretical incompressible results extended to high-subsonic speeds both indicate a thrust for the forebody. The application of transonic approximations, therefore, appears unjustified for similarity parameters less than approximately -1.0 in the subsonic portion of the transonic range.

At lifting conditions and for Mach numbers up to about 0.6, the present results are in good agreement with the closed-tunnel data of Bartlett and Peterson and with low-speed theoretical data extended to a Mach number of 0.6.

The maximum ratio of normal force to drag for the symmetrical double-wedge airfoil was much lower than that for conventional airfoils in the range of Mach numbers below 0.85 and was equal to that for conventional airfoils above a Mach number of 0.85.

Langley Aeronautical Laboratory,
National Advisory Committee for Aeronautics,
Langley Field, Va., August 18, 1954.

REFERENCES

1. Guderley, G., and Yoshihara, H.: The Flow Over a Wedge Profile at Mach Number 1. Jour. Aero. Sci., vol. 17, no. 11, Nov. 1950, pp. 723-735.

2. Trilling, Leon: Transonic Flow Past a Wedge at Zero Angle of Attack. WADC Tech. Rep. No. 52-61 (M.I.T.), Wright Air Dev. Center, U. S. Air Force, Mar. 1952.

3. Habel, Louis W., Henderson, James H., and Miller, Mason F.: The Langley Annular Transonic Tunnel. NACA Rep. 1106, 1952. (Supersedes NACA RM L8A23 by Habel, NACA RM L50E18 by Habel and Henderson, and NACA RM L9G19 by Habel and Miller.)

4. Nelson, William J., and Bloetscher, Frederick: An Experimental Investigation of the Zero-Lift Pressure Distribution Over a Wedge Airfoil in Closed, Slotted, and Open-Throat Tunnels at Transonic Mach Numbers. NACA RM L52C18, 1952.

5. Guderley, Gottfried, and Yoshihara, Hideo: Two-Dimensional Unsymmetric Flow Patterns at Mach Number One. AF Tech. Rep. No. 6683, Wright Air Dev. Center, U. S. Air Force, Jan. 1952.

6. Bartlett, G. E., and Peterson, J. W.: Wind-Tunnel Investigation of Double-Wedge Airfoil at Subsonic Speeds. Bumblebee Rep. No. 53 (Contract NOrd-8993), Cornell Aero. Lab., Aug. 1946.

7. Katzoff, S., Gardner, Clifford S., Diesendruck, Leo, and Eisenstadt, Bertram J.: Linear Theory of Boundary Effects in Open Wind Tunnels With Finite Jet Lengths. NACA Rep. 976, 1950. (Supersedes NACA TN 1826.)

8. Vincenti, Walter G., and Wagoner, Cleo B.: Transonic Flow Past a Wedge Profile With Detached Bow Wave. NACA Rep. 1095, 1952. (Supersedes NACA TN's 2339 and 2588.)

9. Bryson, Arthur Earl, Jr.: An Experimental Investigation of Transonic Flow Past Two-Dimensional Wedge and Circular-Arc Sections Using a Mach-Zehnder Interferometer. NACA Rep. 1094, 1952. (Supersedes NACA TN 2560.)

10. Cole, Julian D.: Drag of a Finite Wedge at High Subsonic Speeds. Jour. Math. and Phys., vol. XXX, no. 2, July 1951, pp. 79-93.

11. Busemann, Adolf: Application of Transonic Similarity. NACA TN 2687, 1952.

12. Allen, H. Julian, and Vincenti, Walter G.: Wall Interference in a Two-Dimensional-Flow Wind Tunnel, With Consideration of the Effect of Compressibility. NACA Rep. 782, 1944. (Supersedes NACA WR A-63.)

TABLE I.- PRESSURE COEFFICIENTS

M = 0.31

Location, percent c	$\alpha = 0^\circ$		$\alpha = 4^\circ$		$\alpha = 8^\circ$	
	Upper surface	Lower surface	Upper surface	Lower surface	Upper surface	Lower surface
2.5	0.165	0.140	-1.235	0.590	-1.135	0.780
5	.095	.060	-.940	.410	-1.160	.605
10	.045	-.020	-.450	.285	-1.185	.465
15	.015	-.005	-.195	.225	-1.165	.390
20	-.020	-.040	-.185	.170	-1.060	.310
25	-.045	-.060	-.190	.130	-.830	.250
30	-.085	-.105	-.220	.075	-.605	.185
35	-.130	-.150	-.255	.020	-.455	.110
40	-.185	-.205	-.305	-.050	-.370	.035
45	-.300	-.310	-.385	-.170	-.340	-.080
50	-.805	-.770	-.790	-.590	-.460	-.490
55	-.280	-.305	-.360	-.200	-.315	-.120
60	-.180	-.200	-.260	-.120	-.260	-.060
65	-.120	-.140	-.185	-.070	-.200	-.040
70	-.085	-.105	-.130	-.035	-.155	-.020
75	-.040	-.065	-.080	-.015	-.120	-.005
80	-.010	-.040	-.040	0	-.080	0
85	.020	0	-.010	.030	-.055	.015
90	.040	.040	.035	.060	-.030	.025
95	.095	.050	.090	.060	.020	.020

M = 0.48

Location, percent c	$\alpha = 0^\circ$		$\alpha = 4^\circ$		$\alpha = 8^\circ$	
	Upper surface	Lower surface	Upper surface	Lower surface	Upper surface	Lower surface
2.5	0.160	0.148	-1.045	0.609	-1.070	0.763
5	.103	.093	-.900	.438	-1.070	.640
10	.060	.045	-.600	.310	-1.070	.500
15	.022	.007	-.242	.235	-1.071	.415
20	-.018	-.029	-.191	.172	-1.069	.340
25	-.050	-.059	-.205	.120	-.990	.280
30	-.095	-.095	-.240	.060	-.865	.205
35	-.142	-.142	-.282	0	-.705	.131
40	-.210	-.210	-.340	-.075	-.540	.048
45	-.328	-.328	-.440	-.195	-.409	-.072
50	-.881	-.857	-.945	-.675	-.380	-.538
55	-.275	-.325	-.395	-.200	-.285	-.108
60	-.195	-.212	-.280	-.130	-.235	-.058
65	-.130	-.140	-.200	-.080	-.187	-.020
70	-.081	-.092	-.140	-.045	-.145	.009
75	-.040	-.050	-.088	-.015	-.101	.015
80	-.003	-.017	-.045	0	-.063	.018
85	.035	.020	0	.030	-.032	.039
90	.075	.060	.045	.050	-.010	.045
95	.120	.100	.090	.070	.028	.045

TABLE I.- PRESSURE COEFFICIENTS - Continued

M = 0.58

Location, percent c	$\alpha = 0^\circ$		$\alpha = 4^\circ$		$\alpha = 8^\circ$	
	Upper surface	Lower surface	Upper surface	Lower surface	Upper surface	Lower surface
2.5	0.170	0.170	-0.997	0.605	-1.030	0.829
5	.105	.095	-.910	.455	-1.035	.665
10	.055	.045	-.705	.343	-1.040	.521
15	.020	.018	-.375	.260	-1.051	.430
20	-.020	-.020	-.210	.195	-1.045	.352
25	-.055	-.055	-.205	.140	-.985	.285
30	-.095	-.095	-.239	.075	-.881	.220
35	-.150	-.150	-.282	.010	-.755	.150
40	-.218	-.218	-.343	-.070	-.600	.060
45	-.353	-.353	-.455	-.200	-.460	-.075
50	-1.010	-.960	-1.000	-.640	-.392	-.585
55	-.319	-.350	-.405	-.220	-.300	-.120
60	-.205	-.123	-.280	-.130	-.242	-.055
65	-.140	-.150	-.200	-.075	-.190	-.020
70	-.090	-.090	-.135	-.035	-.140	.009
75	-.043	-.050	-.075	-.005	-.102	.020
80	-.003	-.019	-.030	.020	-.070	.040
85	.040	.020	.019	.050	-.040	.050
90	.080	.060	.062	.070	-.009	.058
95	.122	.100	.105	.092	.025	.060

M = 0.63

Location, percent c	$\alpha = 0^\circ$		$\alpha = 4^\circ$		$\alpha = 8^\circ$	
	Upper surface	Lower surface	Upper surface	Lower surface	Upper surface	Lower surface
2.5	0.168	0.168	-1.040	0.655	-1.025	0.805
5	.102	.102	-.915	.470	-1.041	.662
10	.065	.060	-.640	.352	-1.049	.525
15	.025	.025	-.320	.268	-1.045	.432
20	-.013	-.013	-.209	.200	-1.035	.355
25	-.050	-.050	-.205	.140	-.980	.285
30	-.095	-.095	-.240	.082	-.892	.220
35	-.148	-.148	-.285	.018	-.775	.142
40	-.220	-.220	-.352	-.070	-.640	.055
45	-.360	-.360	-.470	-.200	-.508	-.085
50	-1.069	-1.069	-1.082	-.790	-.410	-.630
55	-.320	-.370	-.425	-.245	-.327	-.125
60	-.209	-.230	-.290	-.130	-.260	-.065
65	-.138	-.150	-.199	-.075	-.205	-.023
70	-.089	-.095	-.130	-.035	-.152	0
75	-.040	-.050	-.072	-.008	-.109	.015
80	0	-.010	-.020	.025	-.070	.032
85	.040	.028	.025	.050	-.040	.044
90	.081	.069	.072	.075	-.010	.049
95	.135	.109	.111	.100	.020	.045

TABLE I.- PRESSURE COEFFICIENTS - Continued

M = 0.71

Location, percent c	$\alpha = 0^\circ$		$\alpha = 4^\circ$		$\alpha = 8^\circ$	
	Upper surface	Lower surface	Upper surface	Lower surface	Upper surface	Lower surface
2.5	0.195	0.195	-1.095	0.640	-1.099	0.820
5	.130	.120	-.935	.475	-1.100	.671
10	.080	.070	-.635	.355	-1.100	.530
15	.039	.038	-.330	.270	-1.082	.432
20	-.001	-.001	-.229	.202	-1.045	.350
25	-.040	-.040	-.231	.143	-.970	.280
30	-.085	-.085	-.258	.085	-.870	.210
35	-.140	-.140	-.301	.015	-.761	.133
40	-.211	-.211	-.365	-.075	-.635	.037
45	-.332	-.332	-.480	-.220	-.529	-.101
50	-1.135	-1.045	-1.380	-.890	-.449	-.755
55	-.670	-.555	-.481	-.340	-.360	-.190
60	-.235	-.250	-.305	-.135	-.300	-.103
65	-.139	-.150	-.205	-.090	-.242	-.058
70	-.080	-.090	-.135	-.050	-.195	-.028
75	-.035	-.045	-.071	-.020	-.150	-.010
80	.005	.003	-.020	.011	-.109	.005
85	.050	.040	.025	.040	-.075	.011
90	.092	.075	.070	.060	-.045	.016
95	.135	.115	.110	.087	-.015	.015

M = 0.76

Location, percent c	$\alpha = 0^\circ$		$\alpha = 4^\circ$		$\alpha = 8^\circ$	
	Upper surface	Lower surface	Upper surface	Lower surface	Upper surface	Lower surface
2.5	0.205	0.205	-1.152	0.655	-1.580	0.810
5	.148	.138	-.895	.590	-1.510	.680
10	.099	.089	-.505	.365	-1.381	.548
15	.051	.049	-.295	.281	-1.205	.450
20	.010	.010	-.229	.210	-1.111	.370
25	-.030	-.030	-.220	.150	-.899	.299
30	-.070	-.070	-.240	.095	-.715	.227
35	-.120	-.120	-.275	.030	-.590	.155
40	-.180	-.180	-.332	-.055	-.502	.060
45	-.285	-.285	-.430	-.180	-.460	-.090
50	-1.075	-.895	-1.240	-.810	-.718	-.730
55	-.860	-.925	-.720	-.720	-.355	-.345
60	-.500	-.395	-.345	-.180	-.281	-.080
65	-.210	-.185	-.203	-.085	-.225	-.040
70	-.085	-.100	-.121	-.041	-.171	-.012
75	-.025	-.045	-.060	-.010	-.135	.005
80	.018	0	-.011	.015	-.100	.020
85	.059	.040	.030	.040	-.068	.030
90	.091	.071	.072	.065	-.030	.042
95	.130	.101	.115	.090	0	.050

TABLE I.- PRESSURE COEFFICIENTS - Continued

M = 0.81

Location, percent c	$\alpha = 0^\circ$		$\alpha = 4^\circ$		$\alpha = 8^\circ$	
	Upper surface	Lower surface	Upper surface	Lower surface	Upper surface	Lower surface
2.5	0.218	0.200	-1.450	0.650	-1.720	0.815
5	.165	.155	-1.100	.508	-1.570	.690
10	.115	.108	-.200	.390	-1.340	.555
15	.078	.068	-.120	.305	-1.208	.465
20	.030	.030	-.155	.232	-1.143	.380
25	-.008	-.008	-.180	.175	-1.095	.313
30	-.048	-.045	-.210	.120	-1.060	.243
35	-.094	-.092	-.240	.058	-1.030	.170
40	-.148	-.150	-.275	-.020	-.743	.080
45	-.235	-.235	-.348	-.130	-.443	-.045
50	-.950	-.770	-1.050	-.698	-.375	-.660
55	-1.000	-1.125	-1.093	-.888	-.290	-.708
60	-.728	-.718	-.503	-.450	-.255	-.155
65	-.428	-.318	-.343	-.150	-.233	-.040
70	-.205	-.160	-.230	-.045	-.205	-.015
75	-.065	-.070	-.140	-.005	-.180	-.005
80	.010	-.003	-.065	.030	-.155	.013
85	.060	.042	-.003	.050	-.123	.020
90	.100	.080	.050	.070	-.085	.023
95	.135	.120	.100	.092	-.045	.013

M = 0.86

Location, percent c	$\alpha = 0^\circ$		$\alpha = 4^\circ$		$\alpha = 8^\circ$	
	Upper surface	Lower surface	Upper surface	Lower surface	Upper surface	Lower surface
2.5	0.250	0.228	-0.973	0.700	-1.435	0.820
5	.205	.185	-.872	.520	-1.295	.680
10	.158	.148	-.630	.398	-1.100	.553
15	.120	.110	-.105	.318	-.980	.460
20	.078	.075	-.070	.250	-.940	.380
25	.040	.040	-.102	.193	-.908	.315
30	.008	.008	-.135	.140	-.885	.248
35	-.030	-.030	-.170	.085	-.875	.180
40	-.078	-.078	-.203	.015	-.845	.098
45	-.148	-.155	-.260	-.080	-.550	-.010
50	-.780	-.615	-.898	-.580	-.290	-.550
55	-.968	-.985	-.964	-.900	-.258	-.830
60	-.888	-.955	-.458	-.840	-.263	-.760
65	-.780	-.855	-.340	-.725	-.270	-.505
70	-.470	-.355	-.285	-.340	-.270	-.110
75	-.260	-.210	-.240	-.113	-.260	-.015
80	-.110	-.105	-.185	-.003	-.250	0
85	0	-.008	-.132	.040	-.240	-.015
90	.082	.058	-.074	.050	-.220	-.050
95	.130	.112	0	.065	-.205	-.085

TABLE I.- PRESSURE COEFFICIENTS - Continued

M = 0.91

Location, percent c	$\alpha = 0^\circ$		$\alpha = 4^\circ$		$\alpha = 8^\circ$	
	Upper surface	Lower surface	Upper surface	Lower surface	Upper surface	Lower surface
2.5	0.350	0.300	-0.820	0.720	-1.185	0.855
5	.255	.238	-.700	.555	-1.080	.710
10	.200	.195	-.555	.440	-.918	.580
15	.158	.150	-.470	.360	-.813	.495
20	.118	.115	-.345	.295	-.775	.420
25	.085	.085	-.080	.240	-.750	.355
30	.053	.053	-.045	.190	-.738	.295
35	.020	.020	-.065	.140	-.735	.233
40	-.025	-.025	-.097	.080	-.733	.160
45	-.082	-.090	-.155	-.003	-.665	.060
50	-.670	-.518	-.748	-.458	-.420	-.430
55	-.890	-.880	-.880	-.820	-.293	-.788
60	-.870	-.870	-.755	-.790	-.280	-.743
65	-.820	-.845	-.305	-.764	-.280	-.700
70	-.780	-.810	-.234	-.730	-.282	-.663
75	-.705	-.550	-.202	-.695	-.283	-.628
80	-.440	-.302	-.178	-.670	-.280	-.590
85	-.270	-.205	-.155	-.555	-.280	-.550
90	-.135	-.120	-.128	-.210	-.275	-.485
95	-.060	.010	-.078	-.010	-.270	-.360

M = 0.96

Location, percent c	$\alpha = 0^\circ$		$\alpha = 4^\circ$		$\alpha = 8^\circ$	
	Upper surface	Lower surface	Upper surface	Lower surface	Upper surface	Lower surface
2.5	0.520	0.420	-0.665	0.765	-1.035	0.980
5	.302	.285	-.573	.590	-.908	.750
10	.250	.245	-.438	.480	-.775	.623
15	.210	.205	-.368	.410	-.680	.540
20	.173	.173	-.350	.348	-.648	.465
25	.143	.143	-.348	.298	-.628	.405
30	.118	.112	-.265	.250	-.620	.348
35	.088	.082	-.130	.205	-.615	.290
40	.045	.045	-.122	.148	-.615	.223
45	-.008	-.015	-.153	.070	-.565	.133
50	-.550	-.408	-.660	-.355	-.858	-.325
55	-.758	-.750	-.795	-.700	-.713	-.663
60	-.745	-.745	-.790	-.685	-.518	-.628
65	-.738	-.730	-.775	-.665	-.473	-.595
70	-.732	-.722	-.778	-.655	-.475	-.570
75	-.725	-.720	-.532	-.635	-.450	-.545
80	-.718	-.718	-.330	-.610	-.445	-.528
85	-.705	-.705	-.285	-.572	-.440	-.485
90	-.620	-.588	-.265	-.565	-.430	-.463
95	-.390	-.368	-.260	-.488	-.420	-.370

TABLE I.- PRESSURE COEFFICIENTS - Concluded

M = 1.0

Location, percent c	$\alpha = 0^\circ$		$\alpha = 4^\circ$		$\alpha = 8^\circ$	
	Upper surface	Lower surface	Upper surface	Lower surface	Upper surface	Lower surface
2.5	0.465	0.410	-0.574	0.810	-0.875	0.930
5	.370	.350	-.460	.638	-.793	.780
10	.320	.310	-.315	.538	-.655	.668
15	.270	.270	-.255	.465	-.578	.582
20	.240	.238	-.245	.405	-.545	.510
25	.212	.208	-.252	.358	-.530	.450
30	.183	.183	-.230	.315	-.525	.393
35	.153	.153	-.080	.272	-.530	.338
40	.118	.118	-.065	.220	-.538	.272
45	.075	.070	-.092	.145	-.490	.190
50	-.430	-.290	-.550	-.250	-.760	-.250
55	-.620	-.620	-.682	-.580	-.845	-.580
60	-.618	-.618	-.678	-.565	-.833	-.550
65	-.610	-.605	-.670	-.550	-.828	-.523
70	-.605	-.600	-.682	-.542	-.828	-.500
75	-.600	-.598	-.680	-.538	-.833	-.480
80	-.598	-.598	-.680	-.540	-.828	-.460
85	-.598	-.598	-.682	-.510	-.790	-.440
90	-.550	-.545	-.660	-.480	-.695	-.408
95	-.530	-.510	-.638	-.440	-.480	-.320

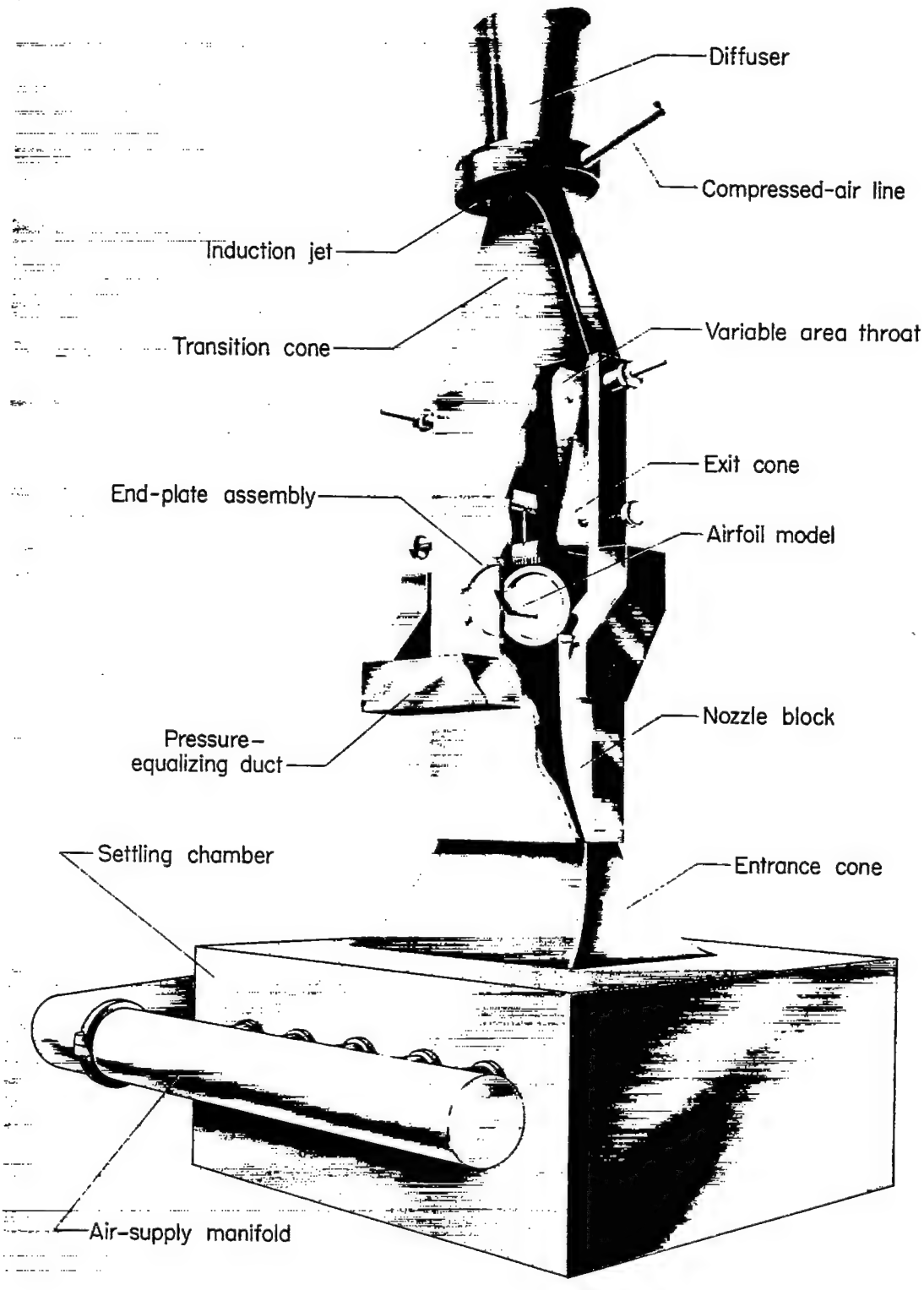

Figure 1.- Langley 4- by 19-inch semiopen tunnel.

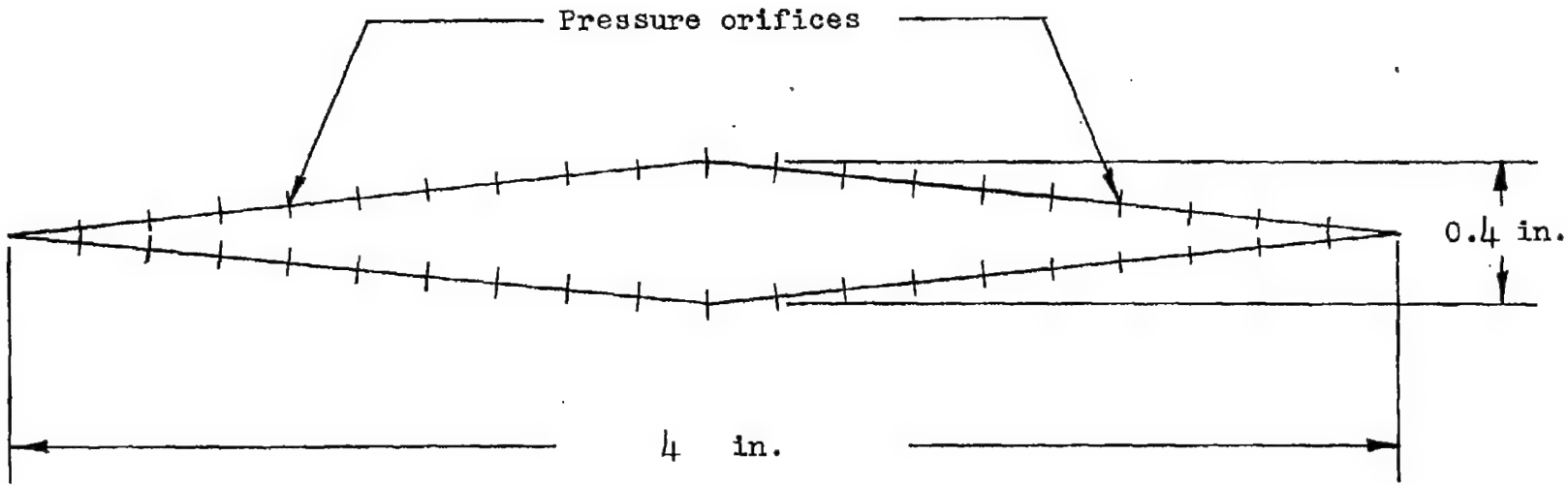

Figure 2.- Profile of the 10-percent-thick symmetrical double-wedge airfoil investigated, showing location of pressure orifices.

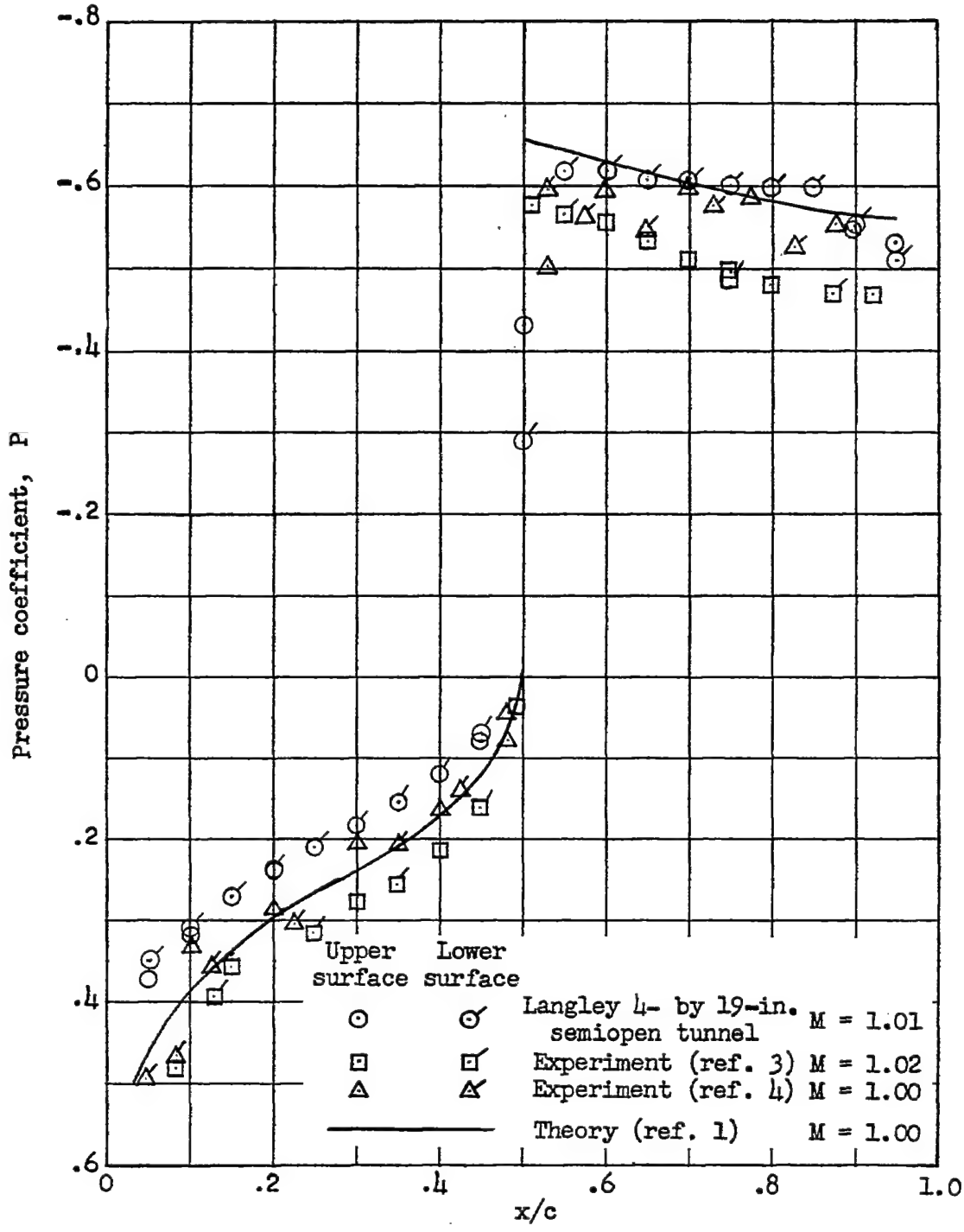

Figure 3.- Comparisons of experimental pressure distributions on a 10-percent-thick symmetrical double-wedge airfoil at zero lift from the Langley 4- by 19-inch semiopen tunnel with those from other facilities.

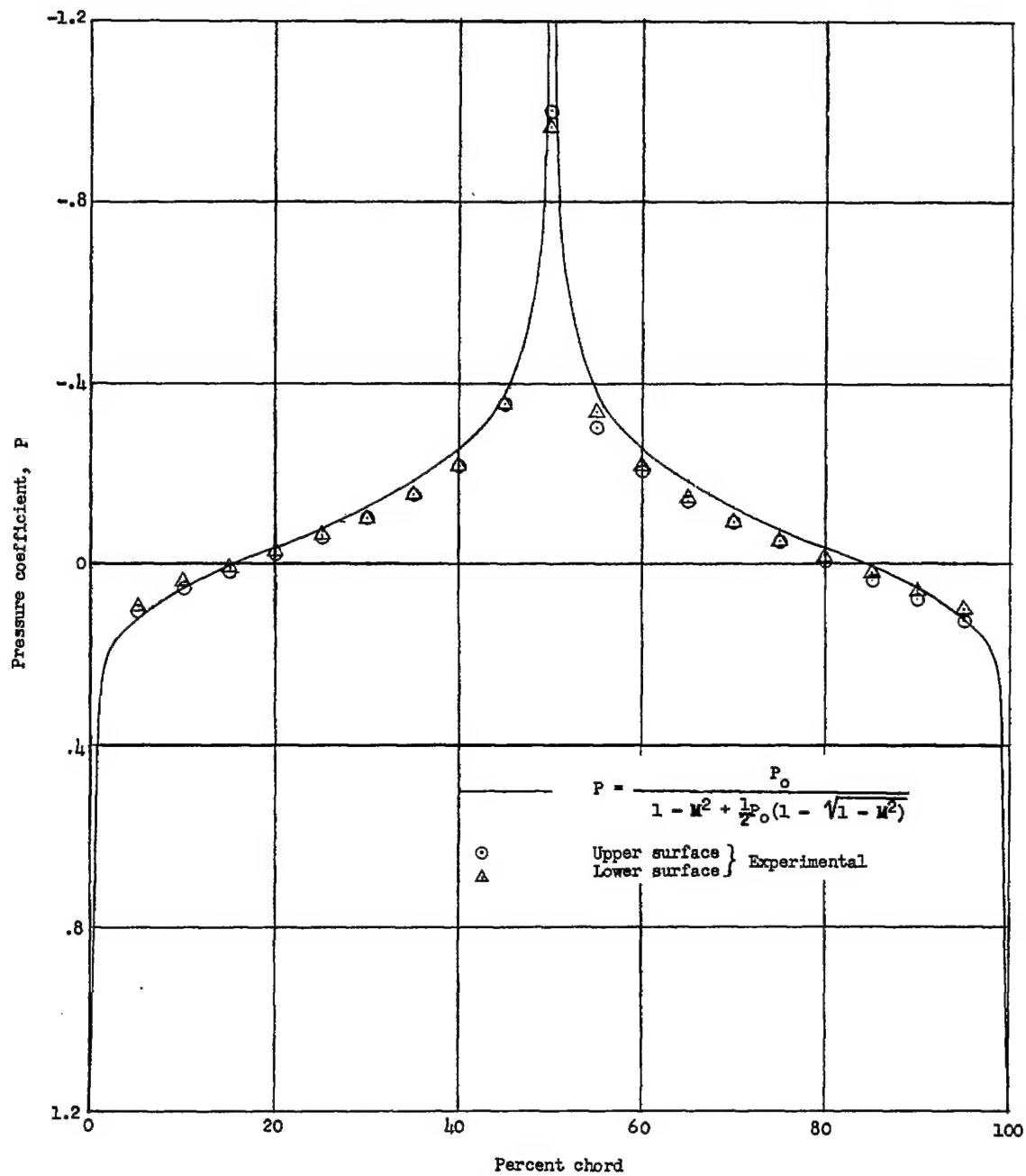

Figure 4.- Comparison of the experimental pressure distribution on a 10-percent-thick symmetrical double-wedge airfoil with extrapolated potential-flow theory at 0° angle of attack and a Mach number of 0.584.

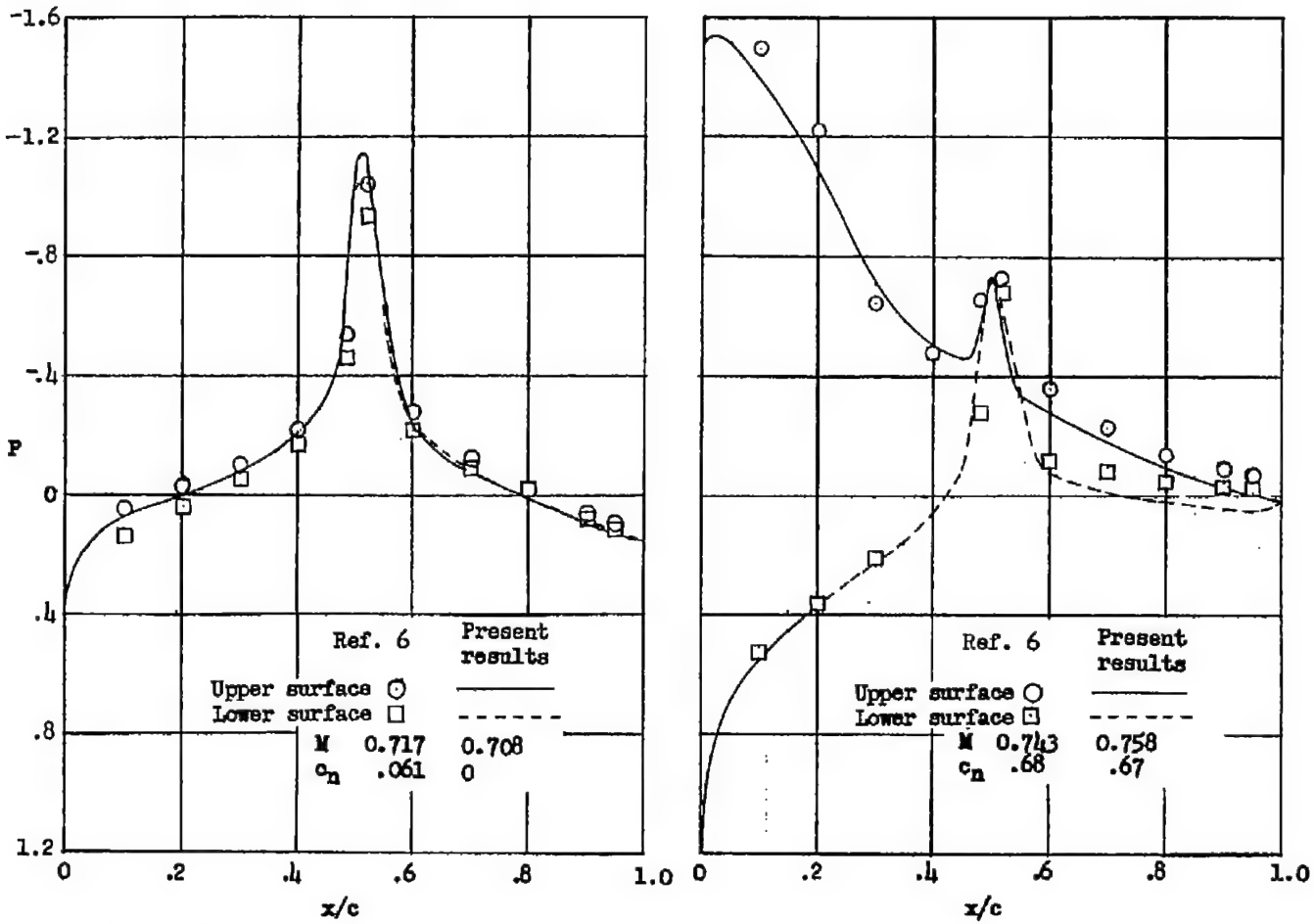

Figure 5.- Comparison of pressure distributions for the 10-percent-thick symmetrical double-wedge airfoil of the present investigation with data from reference 6.

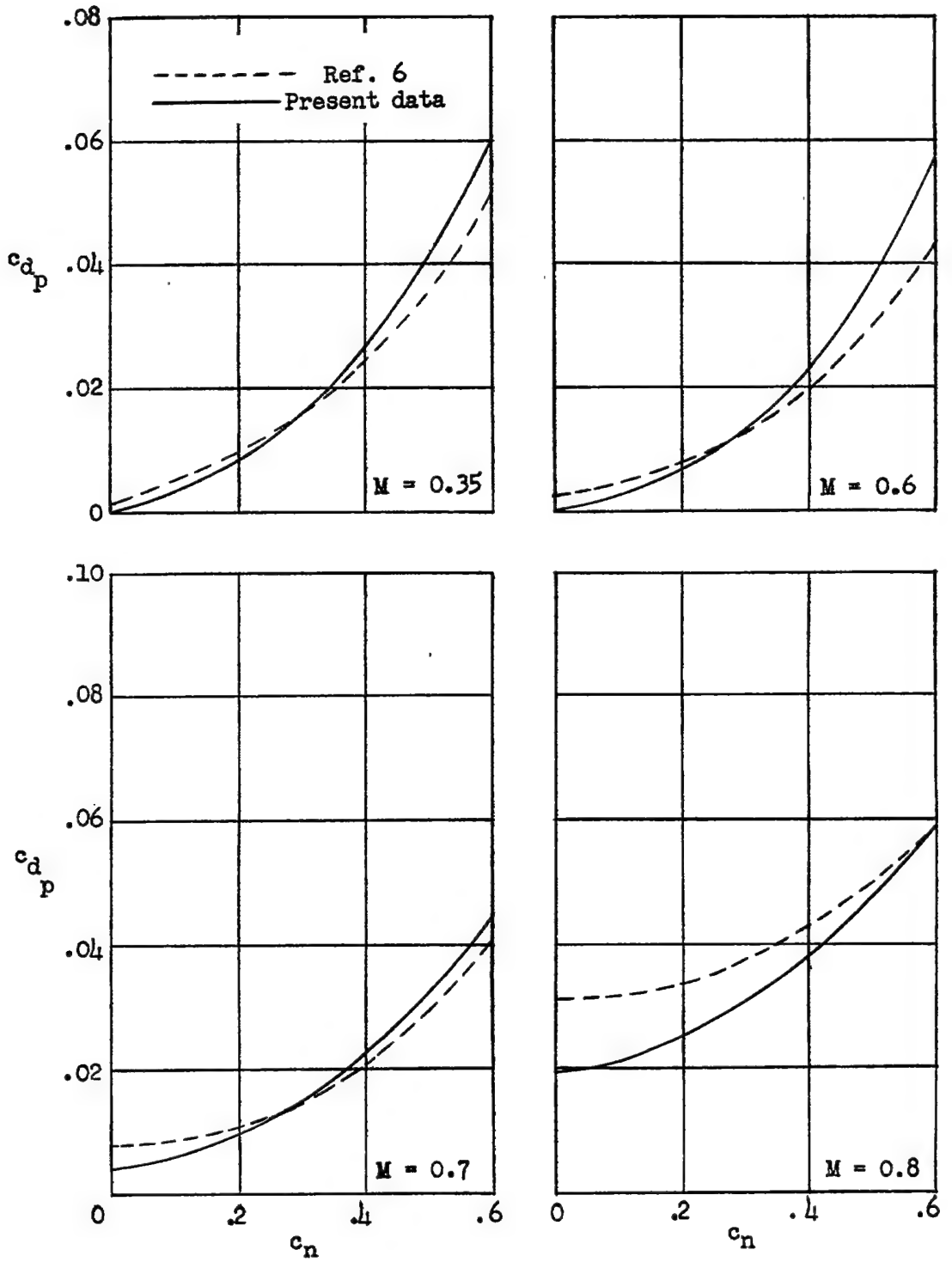

Figure 6.- Comparison of drag polars of the 10-percent-thick symmetrical double-wedge airfoil of the present investigation with data from reference 6.

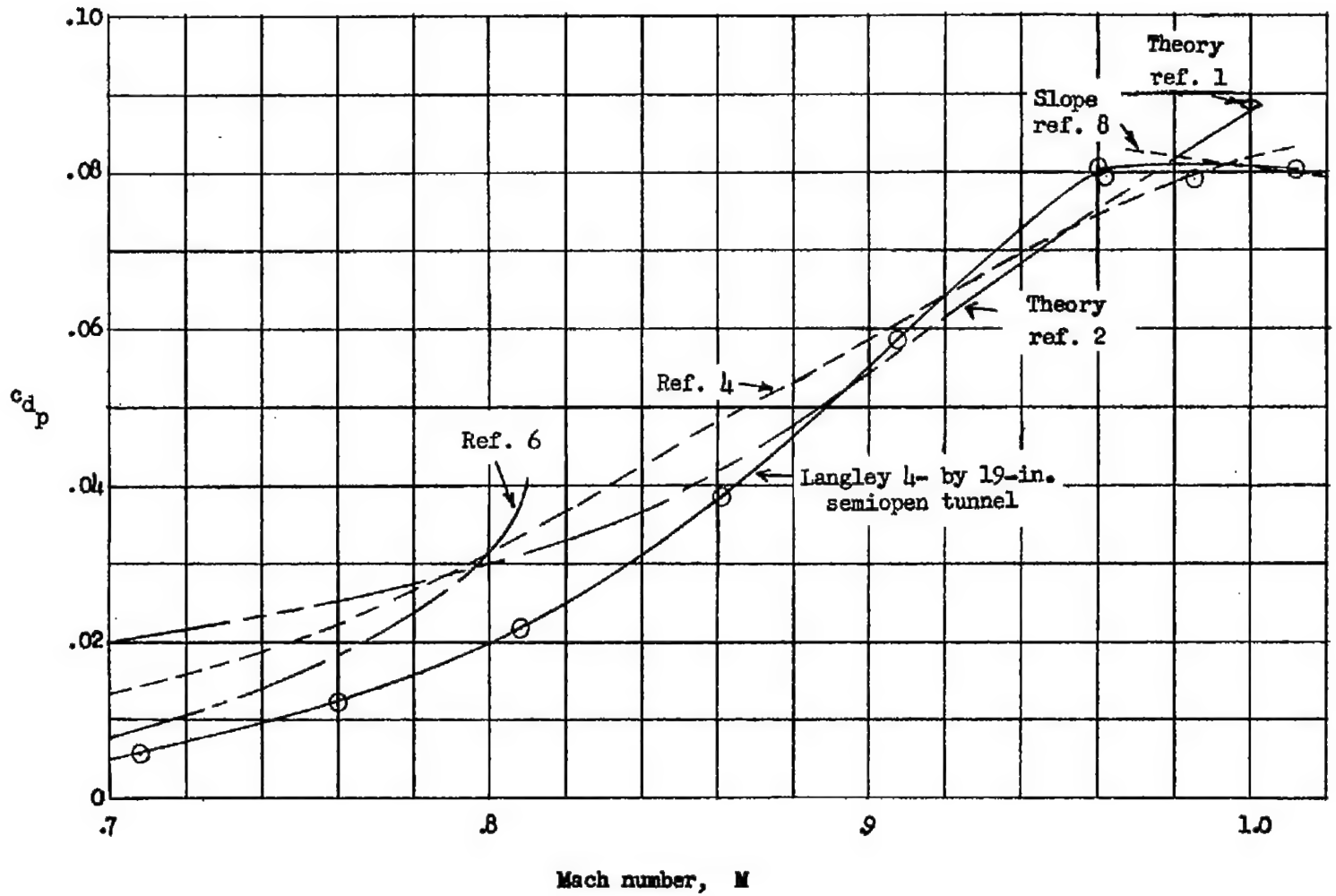

Figure 7.- Comparison of experimental zero-lift pressure-drag coefficients on a 10-percent-thick symmetrical double-wedge airfoil with data obtained in other facilities.

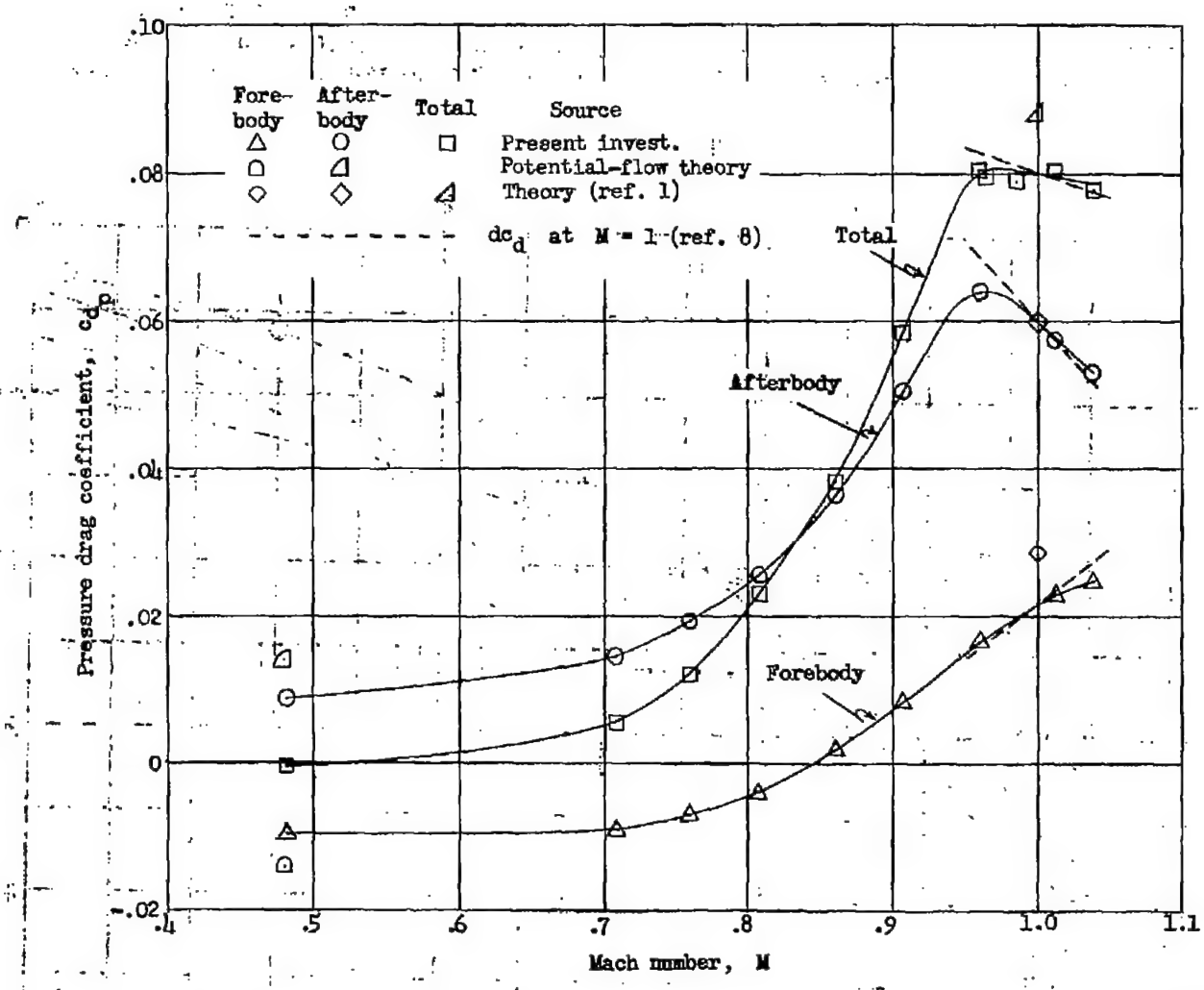

Figure 8.- The components of pressure drag acting on a 10-percent-thick symmetrical double-wedge airfoil in the Langley 4- by 19-inch semi-open tunnel. $\alpha = 0^\circ$.

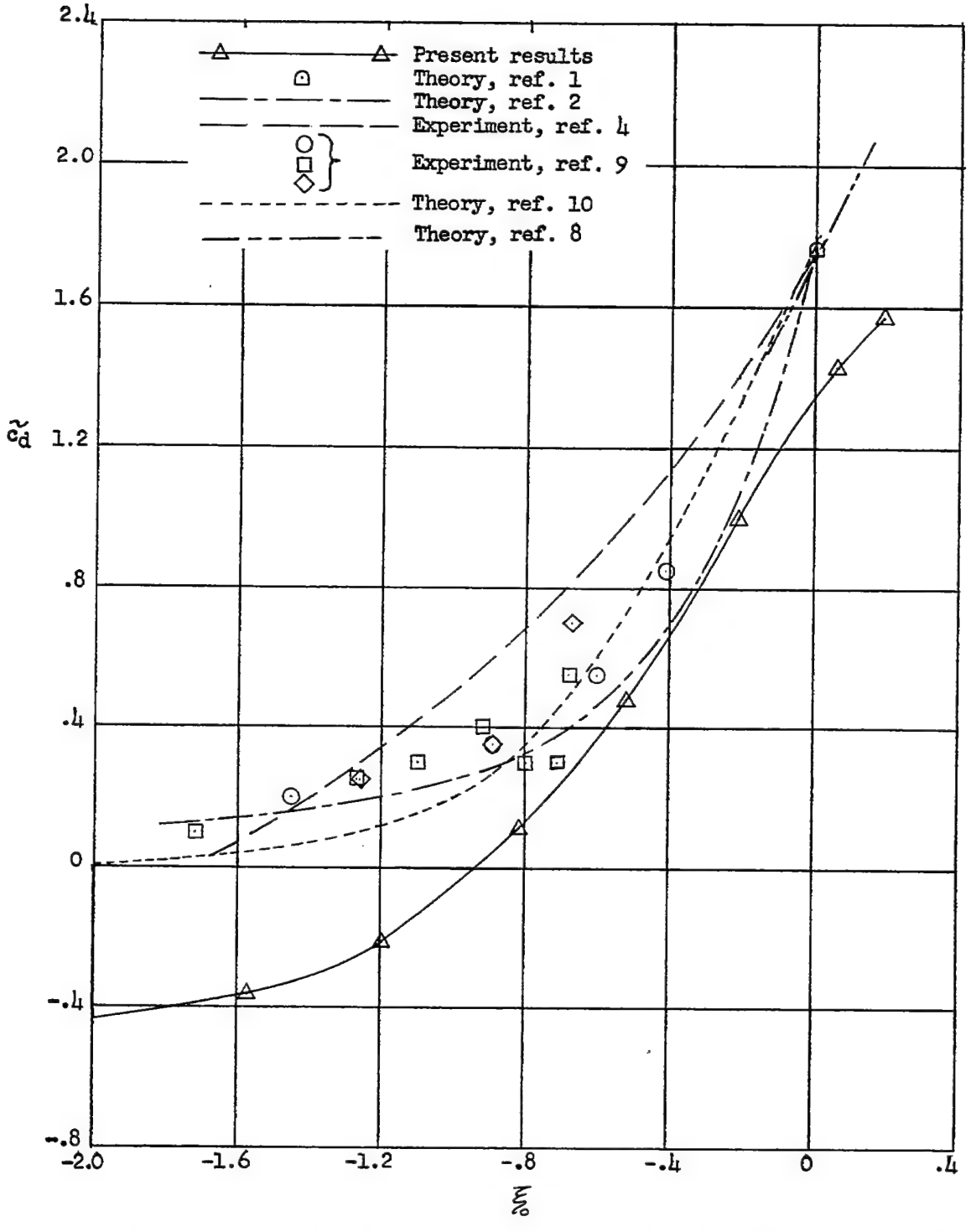

Figure 9.- Experimental and theoretical generalized drag coefficient against reduced Mach number on wedges and on the forebody of symmetrical double-wedge profiles. $\alpha = 0^\circ$.

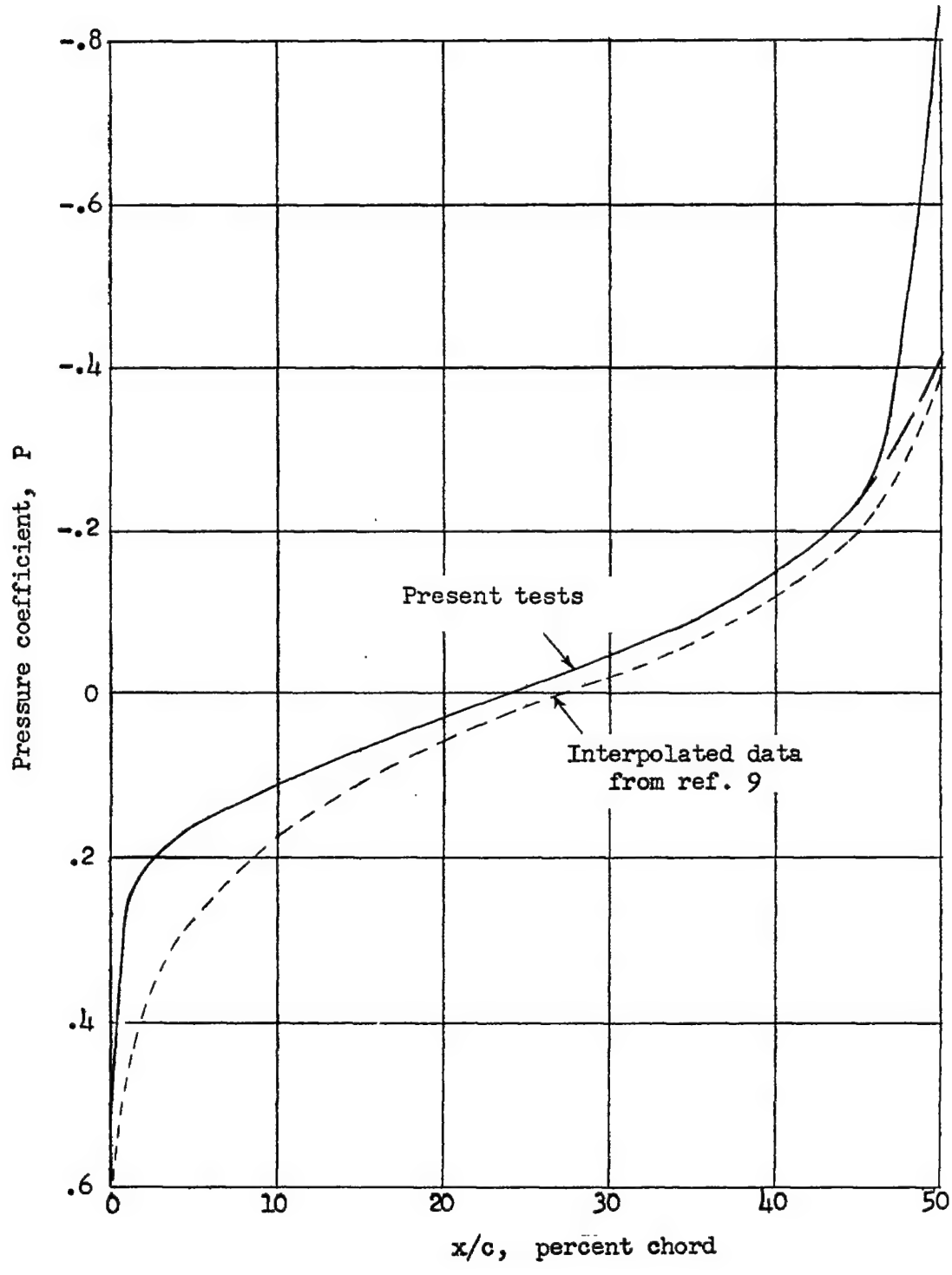

Figure 10.- Pressure distribution for the 5.74° semiangle forebody of the present investigation and the interpolated distribution for a 5.74° semiangle wedge from reference 9. $M \approx 0.82$; $\alpha = 0°$.

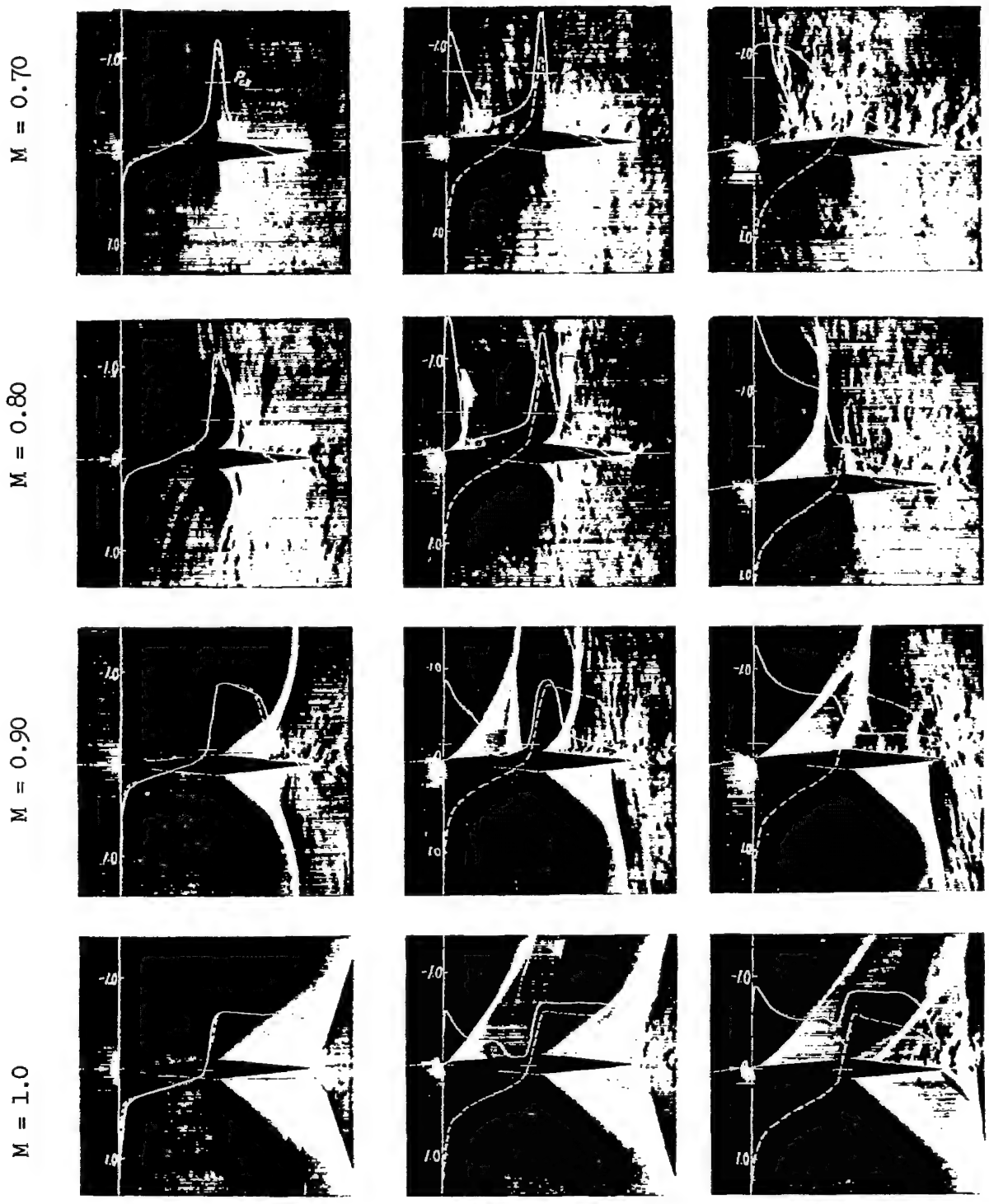

Figure 11.- Flow over 10-percent-thick symmetrical double-wedge airfoil.

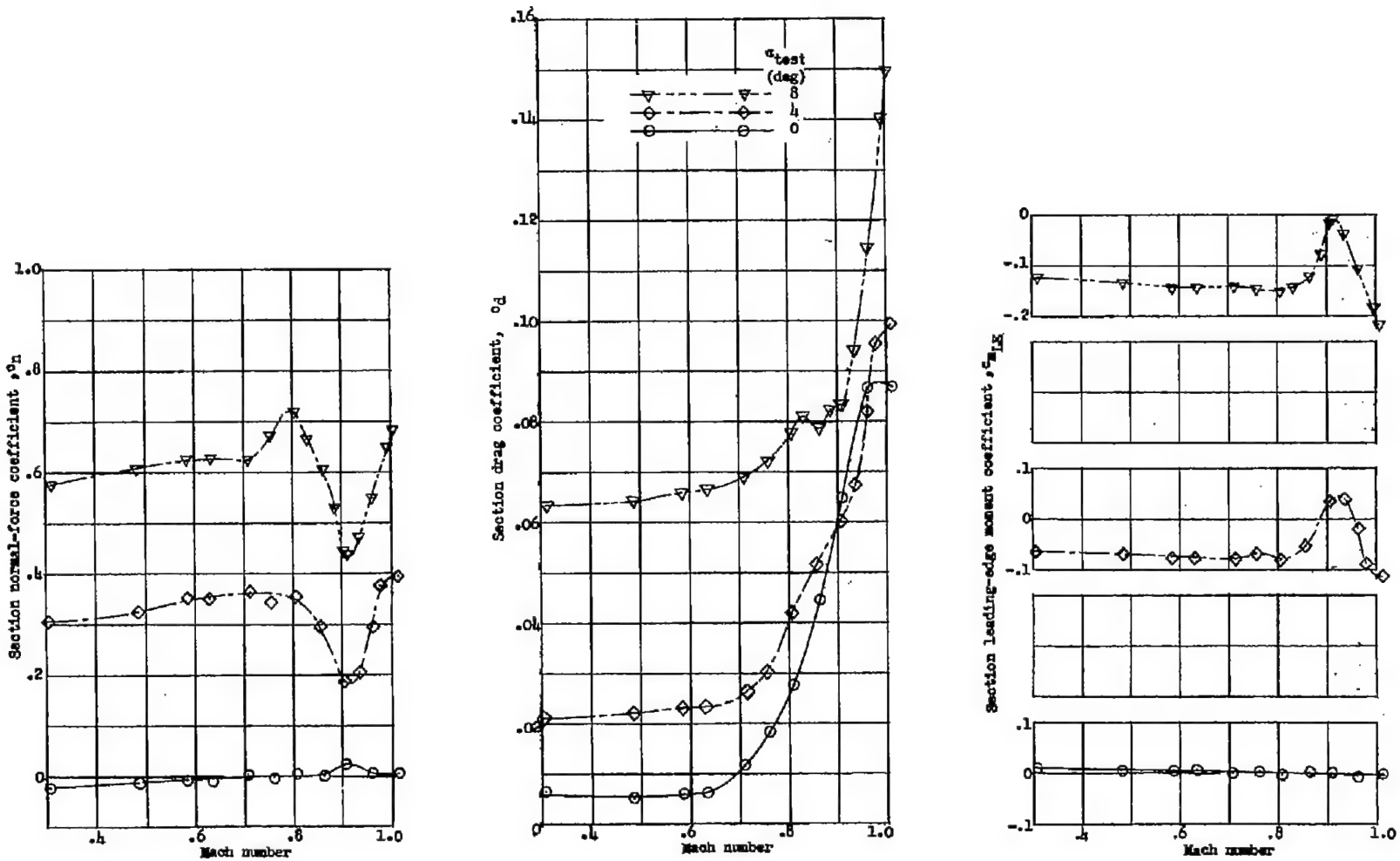

Figure 12.- The aerodynamic characteristics of the 10-percent-thick symmetrical double-wedge airfoil.

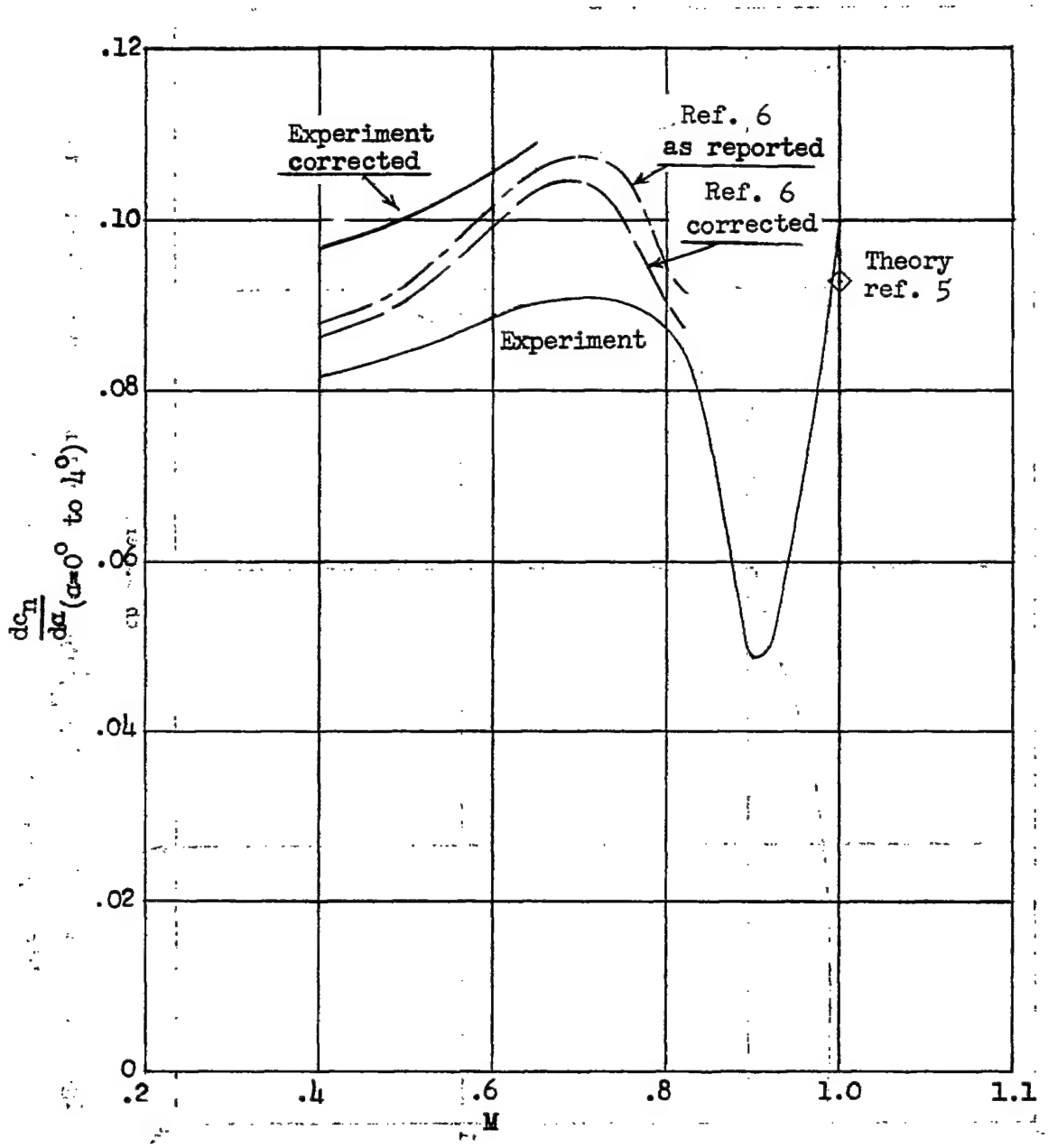

Figure 13.- Comparison of section normal-force-curve slopes on a 10-percent-thick symmetrical double-wedge airfoil.

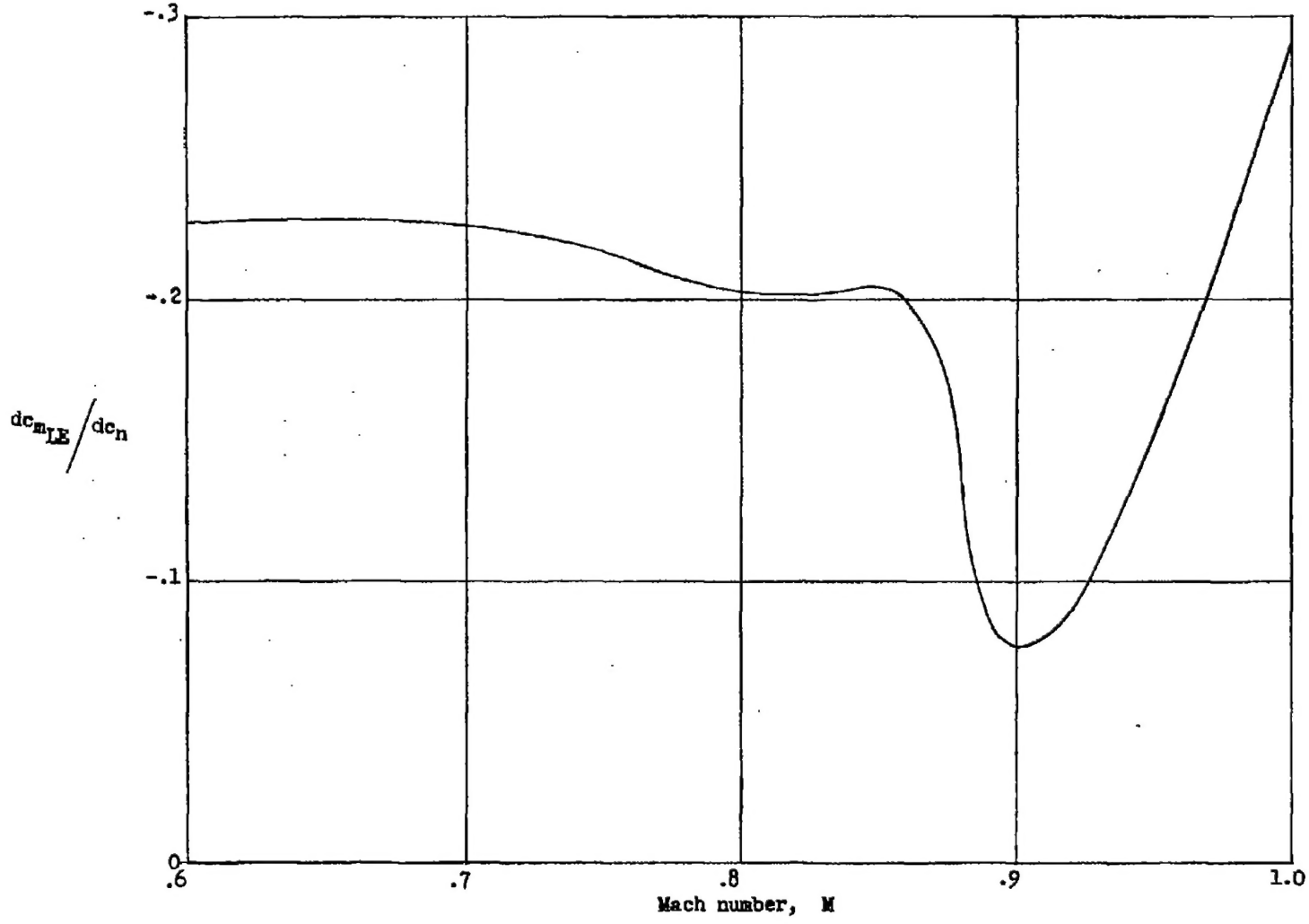

Figure 14.- Variation of $dc_{m_{LE}}/dc_n$ with Mach number on a 10-percent-thick symmetrical double-wedge airfoil. $c_n = 0.3$.

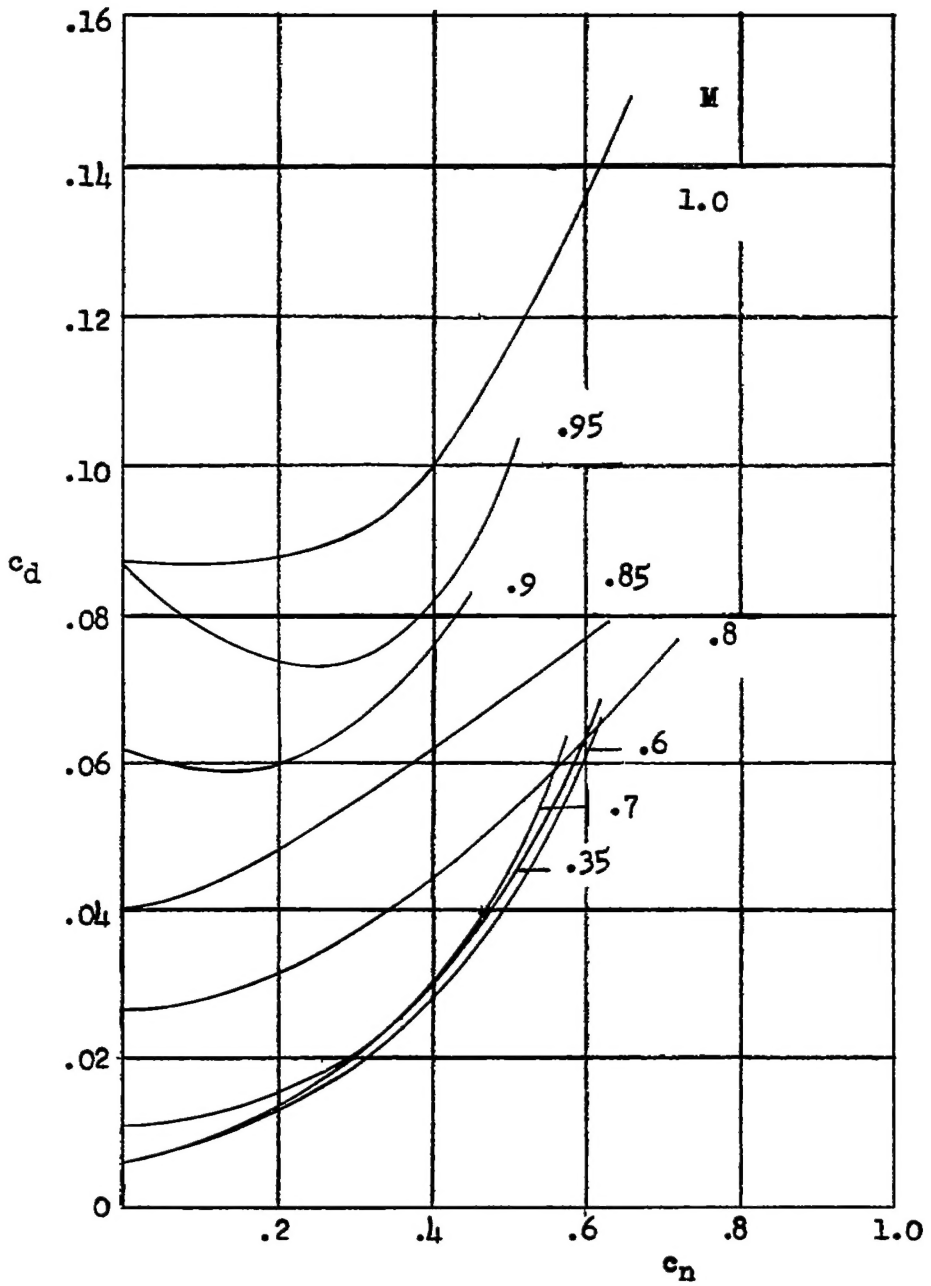

Figure 15.- Variation of section drag coefficient with section normal-force coefficient on a 10-percent-thick symmetrical double-wedge airfoil.

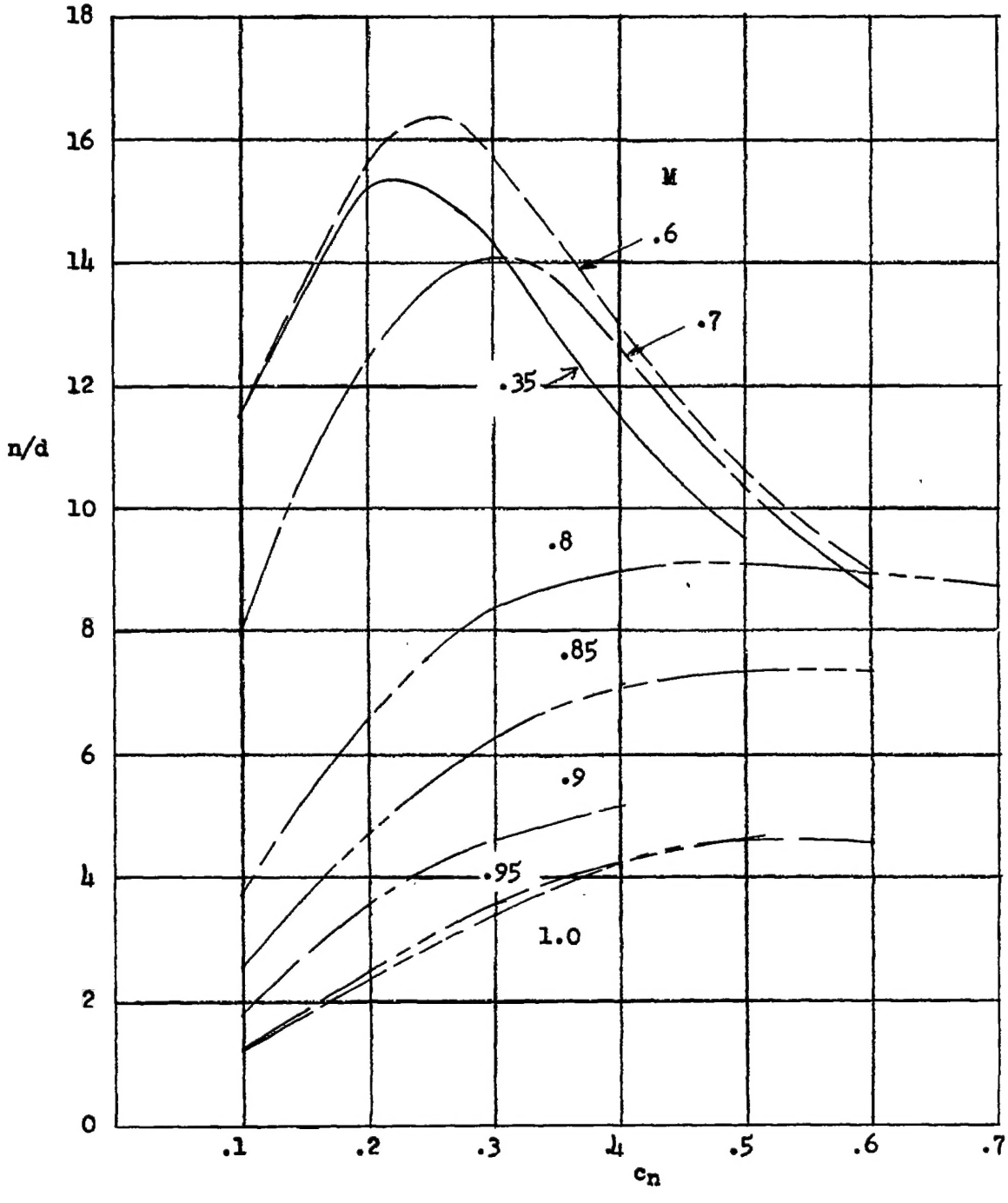

Figure 16.- Variation of ratio of section normal force to drag with section normal-force coefficient on a 10-percent-thick symmetrical double-wedge airfoil.

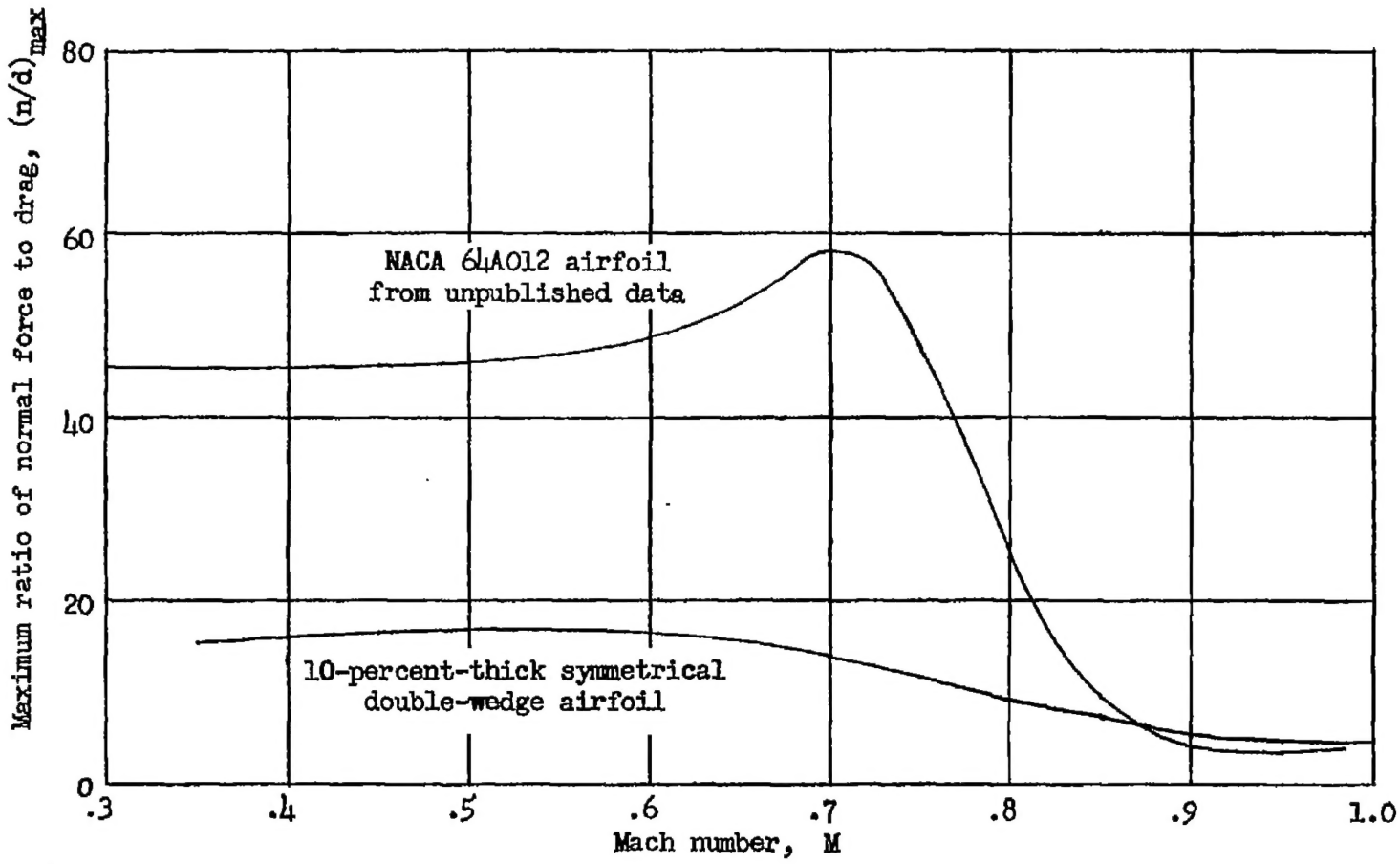

Figure 17.- Maximum ratio of normal force to drag.